ELSEVIER

Contents lists available at ScienceDirect

Sensing and Bio-Sensing Research

journal homepage: www.elsevier.com/locate/sbsr





Eco-friendly electrochemical sensing: An ultra-sensitive voltammetric analysis of ciprofloxacin in human serum, cow's milk and pharmaceutical samples using a glassy carbon electrode modified with poly(Na₂[Cu(HR)₄])

Adane Kassa a,*, Demisachew Shitaw a, Zelalem Bitew c, Atakilt Abebe b

- a Chemistry Department, College of Natural and Computational Sciences, Debre Markos University, P.O. Box 269, Debre Markos, Ethiopia
- ^b Chemistry Department, College of Sciences, Bahir Dar University, Bahir Dar, Ethiopia
- ^c Department of Energy and Process Engineering, Norwegian University of Science and Technology, NO-7491 Trondheim, Norway

ARTICLE INFO

Keywords: Ciprofloxacin Electrochemical determination Glassy carbon electrode Sodium tetra(resorcinate)cupprate (II) Tablet formulations

ABSTRACT

Recent advances in electrochemistry and electrode surface modification highlight the potential of transition metal coordination compounds as effective modifiers. This study presents sodium tetraresorcinolatocuprate(II) (Na₂[Cu(HR)₄]), a newly synthesized compound characterized using UV-Vis, FT-IR spectroscopy, ICP OES, and melting point analysis. A poly(Na₂[Cu(HR)₄])/GCE was fabricated via potentiodynamic techniques, with cyclic voltammetry and electrochemical impedance spectroscopy confirming the formation of a polymer film that enhanced the electrode's active area and electrocatalytic properties. The developed poly(Na₂[Cu(HR)₄])/GCE was applied for determination of ciprofloxacin (CPF), an antibiotic prone to resistance issues, that requires reliable monitoring in pharmaceutical and biological samples. The poly(Na₂[Cu(HR)₄]) modifier significantly improved CPF detection by reducing its oxidation potential and increasing current response by eightfold compared to unmodified electrodes, suggesting the modifier's catalytic role in CPF oxidation. Differential pulse voltammetry (DPV) showed a linear CPF response over concentrations of 1.0×10^{-8} to 4.0×10^{-4} M, with detection and quantification limits of 2.0 nM and 6.8 nM, respectively. Analysis of commercial CPF brands showed 98.05-100.00 % accuracy, while spike recovery rates (99.25-100.40 %) and low interference errors (<4.6 %) validated the developed method for complex samples. The presented method is generally useful for determination of electroactive species in real complex samples and may aid in the design of more efficient electrochemical sensors.

1. Introduction

Ciprofloxacin(1-cyclopropyl-6-fluoro-4-oxo-7-(piperazin-1-yl)-1,4-dihydroquinoline-3-carboxylic acid) (see Scheme SM1A) is a commonly prescribed antibiotic for the treatment of mild-to-moderate bacterial infections, particularly those affecting the respiratory and urinary tracts [1,2]. By interacting with the bacterial DNA gyrase, CPF inhibits DNA synthesis and stops bacterial cell development, exerting its bactericidal effect [3]. However, in addition to its severe side effects a significant resistance issue has arisen despite the drug's considerable success in clinical settings, which has led to the need for a high dosage regimen and a new combination of pharmacokinetics [4,5]. Furthermore, due to its widespread use and the risks it poses to both individuals and the environment, there is a crucial need to create an uncomplicated,

inexpensive, and easy-to-use technique for measuring the concentration of CPF in bodily fluids from patients and clinical samples.

Numerous analytical methods such as chromatography [5], spectrophotometry [6] and LC/MS/MS [7] have been devised for determining CPF in real samples. These techniques are typically costly, require laborious sample pre-treatment, take a long time, and have negative environmental effects. Nowadays, electrochemical approaches have garnered a lot of interest because of their great sensitivity, ease of use, affordability, quick reaction, and environmental friendliness [8. 9].

There are limited studies available on using electrochemical techniques for CPF detection in actual samples [10–14]. Examples of existing electrochemical approaches include high cost modifiers, such as gold nanoparticles [14], which involve intricate preparation steps, and mercury-based electrodes [9], which are environmentally harmful.

E-mail address: adane_kassa@dmu.edu.et (A. Kassa).

^{*} Corresponding author.

Cheap, selective, eco-friendly, and sensitive electrochemical sensors are necessary to quantify CPF in diverse real samples. In this work, we will expand beyond the present knowledge by exploring transition metal complexes as effective modifiers. Transition metal complexes have emerged as potential electrode modifiers, showing promise in enhancing performance by increasing surface area and catalytic activity. Such modifications can significantly improve electrode properties, enhancing selectivity, stability, sensitivity, and reproducibility [8,14–16].

In this regard, copper(II) is identified as a very good starting Lewis acid which undertakes redox activities by switching between +1 and +2 oxidation states in desirable potential ranges in which the selected analyte is investigated. Resorcinol ($C_6H_6O_2$) (H_2R)) (scheme SM1B) has a very weak ligand and poor to coordinate with most transition metal ions. The treatment of resorcinol in a mild aqueous alkaline solution deprotonates proton based on the concentration of the base and consequently, can coordinate with metal ions [15–17].

In this study a new voltammetric method was developed for detecting ciprofloxacin in pharmaceutical formulations, cow milk, and human blood serum using a selective, simple, environmentally friendly, and cost-effective transition metal complex modified electrochemical sensor. The sensor, developed by modifying a glassy carbon electrode with poly(sodiumtetraresorcinatecuprate(II)), utilizes a newly synthesized complex and is fabricated through a single-step process, offering a more streamlined approach compared to conventional electrode modifications.

2. Materials and methods

2.1. Apparatus and chemicals

The equipment/instruments utilized in this study included a CHI 760E potentiostat (Austin, Texas, USA), an Adwa AD8000 pH meter (Romania), a Lec Refrigeration PLC refrigerator (England), a Nimbus electronic balance (ADAM Equipment, USA), a Bante901P portable pH/conductivity/TDS meter, a Cary 60 UV–Vis spectrophotometer (Agilent Technologies), a PerkinElmer BX FT-IR spectrophotometer (PerkinElmer, BX), Atomic absorption spectrophotometer (PerkinElmer, AAnalyst 800), ICP-OES spectrometer (PerkinElmer, Optima 7300 V HF Version), and a Stuart SMP30 melting point apparatus.

The following analytical grade chemicals were employed in this work and used as received without further purification: ciprofloxacin (≥ 99.0 %), AgNO $_3$ (≥ 99.0 %) and acetonitrile (99%) (Sigma Aldrich); CuCl $_2\cdot 2H_2O$ (98%, ACS reagent); methanol (100%), dimethylformamide (>99%), dimethyl sulfoxide (95%), and dichloromethane (>99%) (Loba Chemicals Pvt. Ltd); resorcinol (≥ 99.0 %), $K_3[Fe(CN)_6]$ and $K_4[Fe(CN)_6]$ (98.0%) (BDH Laboratory Supplies, England); Na $_2HPO_4$ and NaH $_2PO_4$ (≥ 98.0 %) and KCl (99.5%) (Blulux Laboratories Pvt. Ltd); HCl (37%), HNO $_3$ (70%), and HClO $_4$ (70%,) (Fisher Scientific); NaOH (extra pure, Lab Tech Chemicals), ethanol (CARLO ERBA Reagents S.A.S, France), and deionized water was obtained from Evoqua Water Technologies water purification system and used for all experiments.

2.2. Procedures

2.2.1. Synthesis of poly(Na₂[Cu(HR)₄])/GCE

A mirror-polished GCE was dipped in a 0.1 M phosphate buffer solution (PBS) at pH 7.0, containing 1.0 mM Na₂[Cu(HR)₄]. The electrode was scanned using cyclic voltammetry within an optimized potential range (-1.2 to +1.8 V) for 20 cycles at a scan rate of 100 mV s⁻¹. Following this, the poly(Na₂[Cu(HR)₄])/GCE, after rinsed with deionized water, was further stabilized in 0.5 M H₂SO₄ within the potential range of -0.80 to +0.80 V until a stable cyclic voltammogram was obtained. The poly(Na₂[Cu(HR)₄])/GCE was air-dried and prepared for further use. The same procedure was applied to modify the GCE with poly(H₂R), poly(NaHR), and electrodeposited Cu(0) from 1.0 mM

solutions of each monomer in pH 7.0 PBS.

2.2.2. Preparation of standard CPF solutions

A 5.0 mM stock solution of CPF was made by dissolving 0.166 g of CPF in 100 mL of deionized water. From this stock solution, working standard solutions were prepared through serial dilution with phosphate buffer solutions (PBS) adjusted to the required pH. PBS of various pHs (pH 4.0-8.5) were prepared by mixing 0.1 M sodium dihydrogen phosphate and disodium hydrogen phosphate solutions.

2.2.3. Pharmaceutical tablet sample preparation

Three brand tablets of Cipro (Remedica Ltd., Cyprus), Ciplet (from Sansheng Pharmaceutical Plc, China), and Brucipro (from an Indian pharmaceutical factory) were purchased from a local pharmacy in Bahir Dar, Ethiopia. Five tablets from each brand were chosen at random, weighing an average of 0.591 g, 0.611 g, and 0.578 g for Cipro, Ciplet, and Brucipro, respectively. The tablets were ground and homogenized using a mortar and pestle.

A 5.0 mM stock solutions of CPF tablet samples were prepared for each brand. This was accomplished by filling a 100 mL volumetric flask with deionized water after transferring a precisely weighed tablet powder equal to 0.166 g (0.191 g for Brucipro, 0.202 g for Ciplet, and 0.196 g for Cipro) of CPF. Working solutions for each brand tablet of CPF were prepared though serial dilution of the stock solutions with pH 6.0 PBS.

Human blood serum samples were obtained from Felege Hiwot Referral Hospital and diluted using PBS at pH 6.0. To conduct recovery analysis, spiked serum samples were prepared by adding varying concentrations of standard CPF (0.0, 20.0, 40.0, 80.0, and 120.0 μ M).

Fresh raw cow's milk was purchased from a local market in Bahir Dar City. To prepare the milk samples, acetonitrile was added to remove proteins, followed by filtration and centrifugation at 4000 rpm for 10 min to eliminate any suspended particles. The resulting clear supernatant was then carefully collected and filtered using a 0.45 μm membrane filter to remove any remaining particulates and diluted with pH 6.0 PBS for electrochemical analysis [15]. Milk samples spiked by various concentrations of standard CPF (0.0, 20.0, 40.0, 80.0, and 160.0 μM) were used for recovery analysis.

2.2.4. Syntheses of the metal complex

A solution of CuCl $_2$ (0.27 g, 2.0 mmol) in 30 mL of ethanol and a solution of sodium resorcinolate (NaC $_6$ H $_5$ O (NaHR)) (0.106 g, 8.00 mmol) were prepared according to a procedure in one of our previously reported works [18]. The resulting mixture was refluxed at 65 °C for 5 h in an oil bath. The reaction mixture was cooled to room temperature, filtered to remove sodium chloride (a side product), and the solvent was evaporated under reduced pressure. The resulting brown powder was recrystallized from ethanol to yield 0.95 g (86.50 %) of the desired product.

2.2.5. Complex characterization procedures

The electrolytic conductance of each species in a 0.1 mM deionized water solution was determined using an Adwa 8000 CE pH meter. UV–Vis electronic spectra were recorded for 1.0 mM solutions of each species (including salts, ligands, and the resulting complex) dissolved in ethanol, using a UV–Vis spectrophotometer within the wavelength range of 200–800 nm. For IR spectral analysis, approximately 0.001 g of each sample was mixed with 0.2 g of KBr to form pellets, and the spectra were measured between 400 and 4000 ${\rm cm}^{-1}$ using an FT-IR spectrophotometer.

To determine the Cu and Na content in the complex, 0.01~g of the synthesized compound was treated with 5.0~mL of concentrated HNO_3 and analyzed using atomic absorption spectroscopy (AAS). The HNO_3 digestion process was repeated three times to ensure the complete removal of organic materials from the complex. The remaining residue was then dissolved and diluted with deionized water to the required

concentration for analysis. The melting points of the compounds were measured using a Stuart SMP30 melting point apparatus.

2.2.6. Electrochemical measurements

Electrochemical measurements were carried out using a three-electrode setup, consisting of an Ag/AgCl (3.0 M KCl) as reference electrode, a bare GCE(3 mm diameter) or poly(Na₂[Cu(HR)₄])/GCE as the working electrode, and a platinum coil as the counter electrode. To evaluate the properties of the modified electrode, electrochemical impedance spectroscopy (EIS) and cyclic voltammetry (CV) were conducted using Fe(CN)₆³-/⁴- as a probe. Additionally, CV and differential pulse voltammetry (DPV) were employed to examine the electrochemical behavior and determine the concentration of ciprofloxacin in real samples at the surface of the poly(Na₂[Cu(HR)₄])/GCE, respectively.

3. Results and discussion

3.1. Synthesis of Na₂[Cu(HR)₄] complex

The novel Na₂[Cu(HR)₄] complex was prepared through a two-step synthesis process, as shown in eq. (1) (Scheme 1), using H_2R , NaOH, and CuCl₂ as starting materials.

3.2. Physicochemical characterizations of the complex

The synthesized complex was soluble in polar solvents like water, DMSO, and ethanol but insoluble in non-polar solvents such as chloroform, acetonitrile, DMF, THF, dichloromethane, and acetone. These properties indicate a polar nature of the complex. It also exhibited a distinct brown color, suggesting a change in composition compared to the original materials. Moreover, the complex decomposed at a temperature of $164\,^{\circ}\text{C}$. In addition to the above properties, the metal content analysis confirmed the expected structure of Cu: found $11.31\,\%$ (calculated $11.64\,\%$) and Na: found $8.01\,\%$ (calculated $8.42\,\%$) as the experimental values of the synthesized complex matched with the calculated values.

Furthermore, the complex demonstrated a molar conductivity of $153 \, \mathrm{Scm}^2 \mathrm{mol}^{-1}$ in an aqueous solution, indicating electrolytic behavior and the presence of freely moving ions upon dissolution. However, the observed conductance was lower than anticipated for three ions, which can be attributed to factors such as the significant molar mass of the complex, the surface area of the anion, and the hydrogen bonding between the solvent water and the hydroxyl part of the ligand. These factors collectively might hinder the mobility of the anion [19].

3.3. Fabrication of poly(Na₂[Cu(HR)₄])/GCE

The key to controlling the thickness of a modifying material during potentiodynamic deposition is to monitor the growth of the peak current and optimize the process by analyzing the electrode's response to a probe solution over multiple scan cycles. Fig. 1 illustrates the current response of a poly(Na₂[Cu(HR)₄])/GCE electrode towards CPF at various polymerization scan cycles (10–35). As the scan cycles increase from 10 to 25, the anodic peak current for CPF initially grows and then decreases with increasing intensity (Inset B of Fig. SM1). This decrease

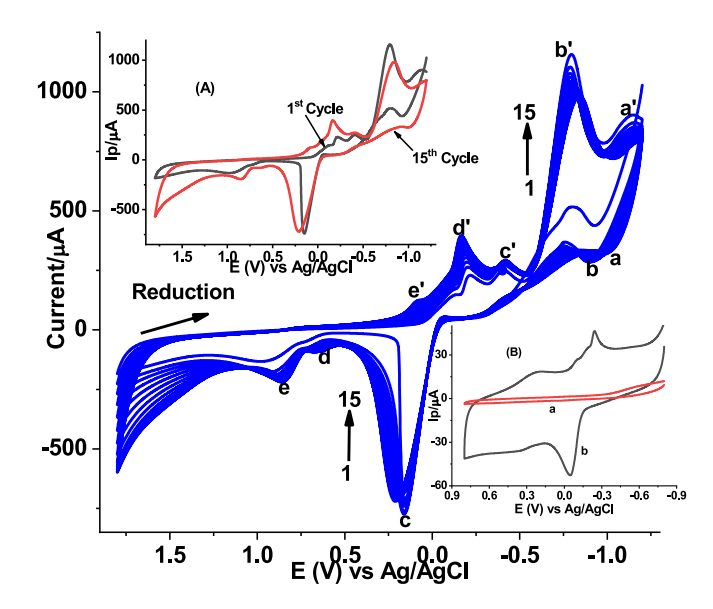


Fig. 1. CVs of GCE recorded repeatedly in pH 7.0 PBS containing 1.0 mM Na₂[Cu(HR)₄], scanned from -1.2 to +1.8 V at a scan rate of 100 mV s⁻¹ over 15 cycles. Inset (A): CVs comparing (a) the bare GCE and (b) the stabilized poly (Na₂[Cu(HR)₄])/GCE, both scanned between -0.8 and +0.8 V at 100 mV s⁻¹ in 0.5 M H₂SO₄. Inset (B): CVs corresponding to the 1st and 15th cycles.

likely indicates saturation of the electrode surface. While increasing the film thickness enhances both current and overpotential, it also extends analysis time. Due to these factors, 15 scan cycles is identified as the optimal polymerization scan cycle in this study (Inset A & B of Fig. SM1).

CVs of GCE in a pH 7.0 PBS containing 1.0 mM $Na_2[Cu(HR)_4]$ are shown in Fig. 1. The potential window for these scans was set between -1.2 V and +1.8 V, and the experiment was repeated for 15 cycles. As the number of cycles increased, both the anodic and cathodic peak currents grew significantly, indicating the successful electrochemical deposition of a poly($Na_2[Cu(HR)_4]$) film on the electrode surface (inset A of Fig. 1). This film formation is further confirmed by the appearance of multiple distinct redox peaks in the CV of the modified electrode (curve b in inset B of Fig. 1), in contrast to the single broad reductive peak observed at the bare GCE (curve a in inset B of Fig. 1). These additional redox peaks are characteristic of the electroactive polymer film, demonstrating its successful immobilization on the GCE surface.

Increasing both the anodic peak (a-e) and cathodic peak currents (a'e') with increasing scan cycles confirmed polymer film deposition at the electrode surface. While the cathodic peaks were speculated to the stepwise reduction of Cu, and the anodic peaks were assigned to the oxidation of Cu [15].

3.4. Electrochemical characterization of poly(Na₂[cu(HR)₄])/GCE

3.4.1. Electrochemical impedance spectroscopy characterization

EIS was employed to evaluate the interfacial electron transfer resistance and confirm that the electrode change was successful. A ferro/ferricyanide redox couple served as the probe for these measurements.

Scheme 1. The path of complex preparation

The Nyquist plots (based on eq. (2)) for both unmodified and modified GCE electrodes showed semicircles at high and low frequencies, along with a 45-degree line at intermediate frequencies, which indicates a diffusion-controlled process. These impedance spectra were analyzed using an equivalent circuit model, as illustrated in the inset of Fig. 2 [14].

$$C_{dl} = \frac{1}{2\pi R_{cl} f} \tag{2}$$

where: $C_{\rm dl}$ stands for the double layer capacitance, f refers to the frequency at which the maximum imaginary impedance (reactance) is observed on the Nyquist plot, and Rct represents the charge transfer resistance, indicated by the diameter of the semicircle in the high-frequency region.

Among the electrodes tested, the poly(Na₂[Cu(HR)₄])/GCE exhibited the lowest charge transfer resistance (Rct = 178.2 Ω , curve e), while the highest resistance was observed for the unmodified GCE (Rct = 5279.9 Ω , curve a) (Table SM1). This suggests that the poly(Na₂[Cu(HR)₄]) film on the GCE surface significantly reduced the charge transfer resistance, thereby enhancing the electron transfer rate between the substrate and the analyte. The improvement can be attributed to the conductive properties of the polymer film, which minimize electrostatic repulsions with the redox probe.

3.4.2. Cyclic voltammetric characterization

CV was employed to monitor the synthesis of a new material by analyzing the voltammograms obtained using $Fe(CN)_6^{3-/4}$ and CPF as redox probes. Figure SM2 displays the repetitive CVs of a GCE in solutions containing Cu(II) salt, H_2R , NaHR, and $Na_2[Cu(HR)_4]$. During each polymerization cycle, distinct oxidative and reductive peaks were observed, indicating the conversion of the salt and ligand into intermediate species and, ultimately, the formation of the desired complex.

To assess the impact of surface modification on the electrode surface area, cyclic voltammetry was performed using $Fe(CN)_e^{3-}/^{4-}$ as the redox probe (Fig. SM3). The active surface areas of the working electrodes were determined by plotting the peak current (I_{P^a}) against the square root of the scan rate $(v^1/^2)$ of the CV response for $Fe(CN)_e^{3-}/^{4-}$, and applying the Randles–Ševčík equation (eq. 3) [20]. This approach

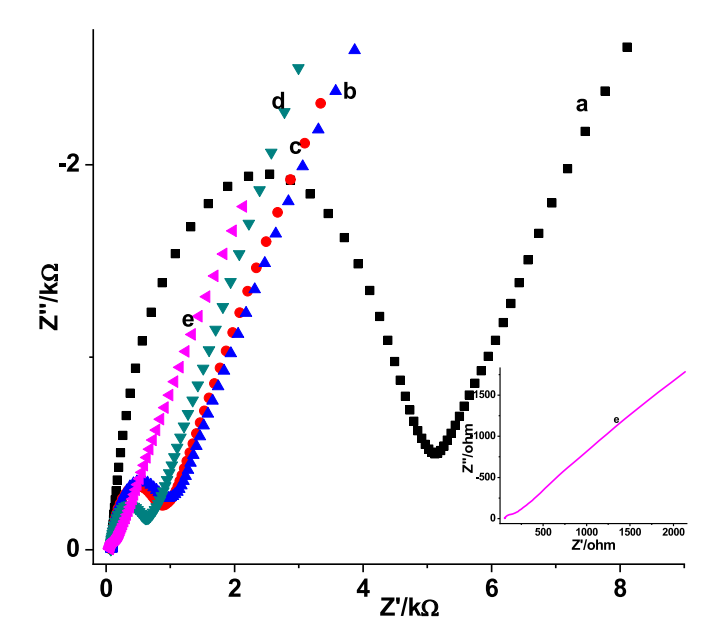


Fig. 2. Nyquist plot for (a) bare GCE, (b) Cu(0)/GCE, (c) poly(H_2R)/GCE, (d) poly(NaHR)/GCE, and (e) poly(Na₂[Cu(HR)₄])/GCE in pH 7.0 PBS containing 10.0 mM [Fe(CN)₆]^{3-/4-} and 0.1 M KCl. Frequency range: 0.01 to 100,000 Hz; amplitude: 0.01 V.

also provided insights into how different surface modifications influenced the electrode's characteristics.

$$I_{pa} = 2.69 \times 10^{5} n^{3/2} A D^{1/2} \nu^{1/2} C_{o}$$
 (3)

where: I_{P^0} represents the anodic peak current, n is the number of electrons transferred (n = 1), A denotes the active surface area of the electrode, D is the diffusion coefficient of $\text{Fe(CN)}_6{}^{3-}/^{4-}$ (D = 7.6 \times 10 $^{-6}$ cm $^2/s$), Co is the bulk concentration of the probe (Co = 10.0 mM), and ν refers to the scan rate.

The effective surface area of each electrode was calculated and is presented in Table 1. The poly(Na₂[Cu(HR)₄])/GCE exhibited a significantly larger effective surface area, approximately 5.5 times greater than that of the unmodified GCE. This increased surface area accounts for the higher current observed for the redox probe, as shown in Fig. SM3. The enhanced electrocatalytic activity of the modified electrode, resulting from the greater number of active sites, contributes to the improved detection of CPF.

Fig. 3 shows the cyclic voltammetric response of the Fe(CN)₆³-/⁴-redox couple at various modified and unmodified GCE electrodes. Compared to the bare GCE, the modified electrodes displayed a pair of well-defined redox peaks with significantly higher current intensity and smaller peak-to-peak potential separation. The current response was in the following order: poly(Na₂[Cu(HR)₄])/GCE > poly(NaHR)/GCE > poly(H₂R)/GCE > poly(Cu(0))/GCE > unmodified GCE. Similarly, the peak-to-peak potential separation (Δ E) showed the trend: poly(Na₂[Cu(HR)₄])/GCE (Δ E = 96 mV) < poly(NaHR)/GCE (Δ E = 106 mV) < poly(H₂R)/GCE (Δ E = 114 mV) < poly(Cu(0))/GCE (Δ E = 187 mV) < unmodified GCE (Δ E = 467 mV). These findings suggest that the poly (Na₂[Cu(HR)₄])/GCE electrode exhibited the best electrochemical performance, indicating that it has the most efficient electron transfer kinetics for the redox probe.

The electrode surface roughness (R_F) , which is a measure of the surface area enlargement of the poly $(Na_2[Cu(HR)_4])/GCE$, can be calculated using eq. (4) as described in reference [15].

$$R_F = \frac{C_{dl}}{C_s} \tag{4}$$

where: C_{dl} and C_{s} denote the electrochemical double-layer capacitance of the planar and smooth electrode surfaces, respectively, made from the same material and measured under identical conditions.

By examining the slopes values for both the unmodified and poly $(Na_2[Cu(HR)_4])$ modified GCE surfaces (Figures SM3A and SM3E), a roughness factor of 5.5 was calculated for the modified electrode compared to the bare GCE. Thus, the substantial increase in surface area indicates that the $poly(Na_2[Cu(HR)_4])$ modified electrode has the potential to serve as a highly sensitive electrochemical sensor, especially for CPF detection.

3.5. Spectroscopic characterization of the synthesized complex

3.5.1. UV-Vis spectral study

A red shift of the π - π^* transition band from 274 nm to 295 nm indicates the deprotonation of H_2R , forming the HR- ion (Fig. 4B). A new band appears at 450 nm, attributed to the n- π^* transition of the C=C-O

 Table 1

 Summary of calculated effective surface area of different working electrodes.

Electrode	Slope of $(\nu)^{1/2}$ vs Ipa	Electrode surface area /cm²
GCE (A)	4.5	0.061
poly(Cu(III))/GCE (B)	8.1	0.11
poly(reso)/GCE (C)	12.4	0.17
poly(NaHR)/GCE (D)	13.4	0.182
poly(Na ₂ [Cu(HR) ₄])/GCE (E)	24.9	0.338

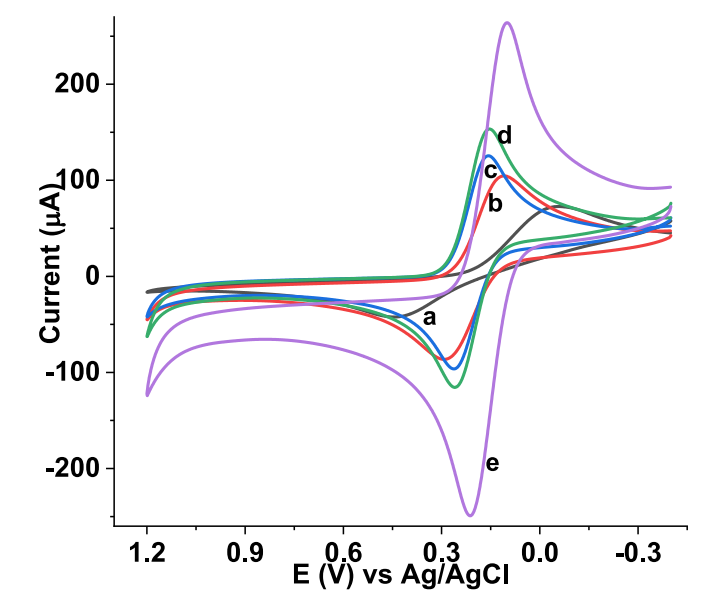


Fig. 3. CVs of (a) GCE, (b) electrodeposited Cu(0)/GCE, (c) poly(H₂R)/GCE, (d) poly(NaHR)/GCE, and (e) poly(Na₂[Cu(HR)₄])/GCE in pH 7.0 PBS containing 10.0 mM (Fe(CN)₆)^{3-/4-} and 0.1 M KCl at scan rate of 100 mV s^{-1} .

group in the deprotonated species (Fig. 4C). The disappearance of the band at 454 nm in the complex's spectrum suggests the involvement of the lone pair of electrons on the deprotonated HR- in coordinating with the Cu(II) ion. The disappearance of the ligand-to-metal charge transfer (LMCT) bands of CuCl $_2$.2H $_2$ O at 292 nm and the d-d transition bands at 624 and 640 nm indicates the formation of a new complex (Fig. 4A). The emergence of a new band at 313 nm in the complex's spectrum is

attributed to a metal-to-ligand charge transfer (MLCT) transition, further confirming the coordination of HR- to Cu(II) (Fig. 4D)'.

3.5.2. FT-IR

The conversion of H₂R is well-documented by the noticeable differences observed in the spectra of the two compounds (Fig. 5A). In the spectrum of H_2R , the band associated with $\nu(OH)$ appeared at 3262 cm⁻¹, but in the spectrum of NaHR, it blue-shift to 3457 cm⁻¹. Additionally, the band at 1606 cm $^{-1}$ corresponding to ν C=C in the H₂R spectrum experienced a slight blue shift to 1614 cm⁻¹, which can be attributed to the increase in electron density within the ring after deprotonation. However, the band at 1488 cm⁻¹, assigned to the C=C bond attached to oxygen, showed a red shift and weakened, appearing at 1474 cm⁻¹. Furthermore, the band at 1160 cm⁻¹ corresponding to vC-O exhibited a red shift to 1146 cm⁻¹. The presence of HR- in the complex is convincingly supported by the observation of its characteristic bands at 3451, 1626, 1539, and 1247 cm⁻¹, corresponding to ν OH, ν C=C, ν C=C-O, and ν C-O, respectively, in the spectrum of the complex (Fig. 5B). The blue shift observed after coordination to Cu(II) can be attributed to an increase in bond order within the benzene ring due to the flow of electron cloud from the filled t_{2g} orbitals of the metal center. Furthermore, the appearance of a new band at 506 cm⁻¹, assigned to Cu—O, further strengthens this argument (Fig. 5B).

3.6. Cyclic voltammetric analysis of CPF

3.6.1. Electrochemical behavior of CPF at poly(Na₂[Cu(HR)₄])/GCE

The combination of low charge transfer resistance (Rct), high surface roughness, and the catalytic properties of the poly(Na₂[Cu(HR)₄]) film results in a highly efficient electrode for CPF oxidation. The catalytic effect of the poly(Na₂[Cu(HR)₄]) film was assessed by comparing the CPF oxidation behavior at both unmodified and modified GCEs using

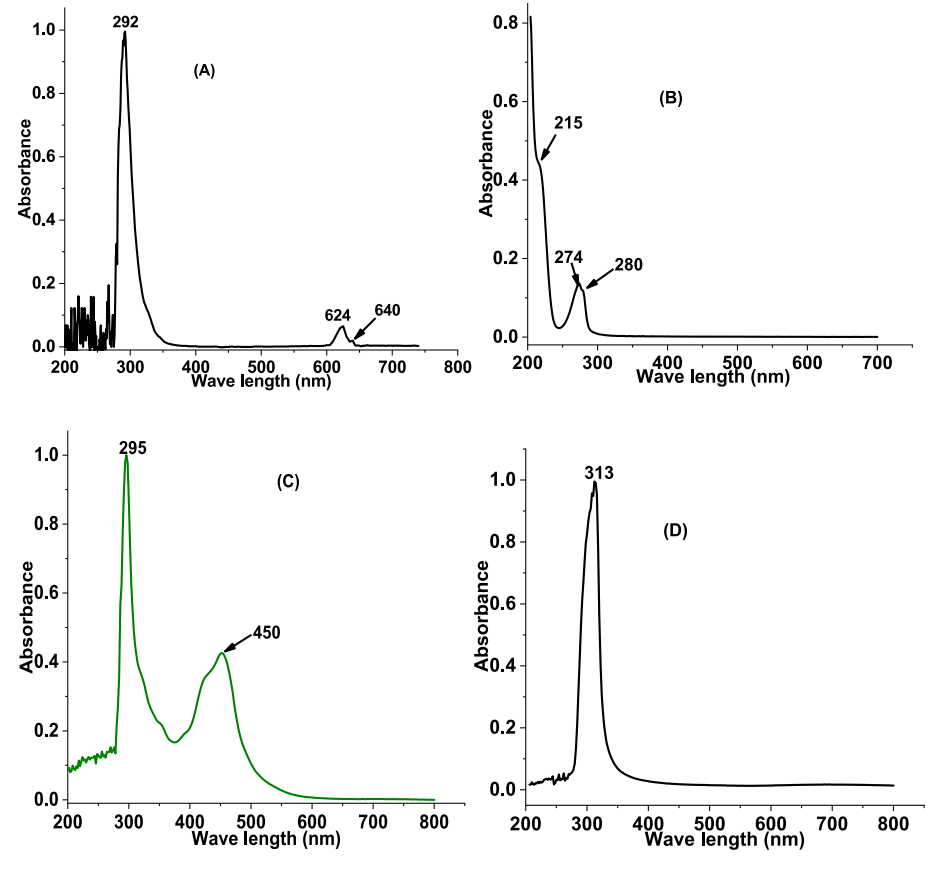


Fig. 4. UV-Vis spectra of (A) CuCl₂.2H₂O, (B) H₂R (C) NaHR, and (D) Na₂[Cu(HR)₄] in ethanol.

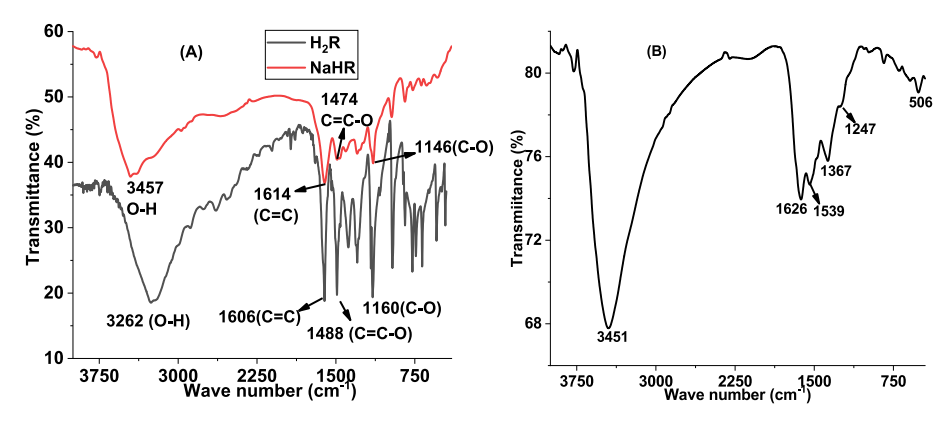


Fig. 5. FT-IR spectra for (A) H₂R, & NaHR, and (B) Na₂[Cu(HR)₄].

cyclic voltammetry. CPF exhibited irreversible oxidation at both electrodes, though with differences in current intensity and peak potential (Fig. 6). A well-defined oxidative peak was observed at a significantly reduced potential ($\Delta E = 188 \, \text{mV}$) and with more than a six-fold increase in current intensity at poly(Na₂[Cu(HR)₄])/GCE (curve b of inset), compared to the unmodified GCE (curve a of inset). The observed peak enhancement and reduced potential confirmed the catalytic activity of the poly(Na₂[Cu(HR)₄]) film towards CPF oxidation, demonstrating the suitability of poly(Na₂[Cu(HR)₄])/GCE for CPF determination in real samples.

3.6.2. Effect of supporting electrolyte on CPF

In this study, several commonly used supporting electrolytes, including phosphate buffer (PBS), acetate buffer (ABS), and Britton-Robinson buffer solution (RBS), were evaluated for their buffering capacity at around pH 5.0 [15]. PBS at pH 5.0 produced a clear oxidative peak with a higher peak current and a lower potential for CPF, as shown in Fig. SM4. Based on these results, PBS, prepared by mixing equimolar (0.1 M) NaH₂PO₄ and Na₂HPO₄, was selected as the supporting electrolyte for further experiments.

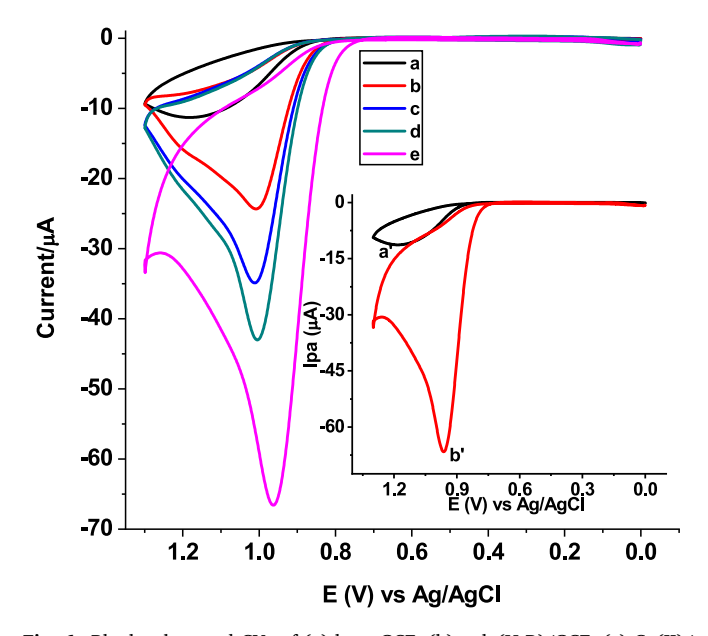


Fig. 6. Blank-subtracted CVs of (a) bare GCE, (b) poly(H_2R)/GCE, (c) Cu(II)/GCE, (d) poly(NaHR)/GCE, and (e) poly(Na₂[Cu(HR)₄])/GCE in pH 7.0 PBS containing 0.5 mM CPF at scan rate of 100 mV s⁻¹. Insets: blank-corrected CVs for (a') unmodified GCE and (b') poly(Na₂[Cu(HR)₄])/GCE.

3.6.3. Effect of pH on peak potential and peak current

The influence of PBS pH on the oxidation peak potentials and peak currents of CPF at the surface of poly(Na₂[Cu(HR)₄])/GCE was explored over a pH range of 4.0 to 8.5. This investigation aimed to determine the involvement of protons in the reaction, assess the electron-to-proton ratio, and understand the interaction between CPF and the electrode surface. The observed shift in the oxidative peak potential with a negative shift across the pH range from 4.0 to 8.5 indicated proton involvement in the CPF reaction at the poly(Na₂[Cu(HR)₄])/GCE surface (Fig. 7A). The slope of 0.043 for the plot of oxidative peak potential versus pH (curve b in Fig. 7B) confirmed a 1:1 electron-to-proton ratio

The CPF oxidation peak current increased with pH from 4.0 to 6.0, then decreased at pH values above 6.0 (curve b in Fig. 7B), suggesting that pH 6.0 was optimal. This current trend can be attributed to Coulombic interactions between the poly(Na₂[Cu(HR)₄])/GCE film (with a pKa value of 9.15) [15] and CPF (pKa: 6.1 and 8.6) [22]. The increasing peak current from pH 4.0 to 6.0 likely results from the attraction between the cationic form of CPF (pKa 6.1) and the negatively charged modifier film. Therefore, pH 6.0 was selected as the optimal PBS pH for subsequent experiments.

3.6.4. Effect of scan rate on Ipa and Ep of CPF

To investigate the reversibility of the oxidation reaction and further understand the reaction kinetics during CPF oxidation, the effect of scan rate on the peak current (I_{P^a}) of CPF was examined. Cyclic voltammograms of poly($Na_2[Cu(HR)_4]$)/GCE in pH 6.0 PBS containing 0.5 mM CPF were recorded at scan rates ranging from 10 to 300 mV s⁻¹, as shown in Fig. 8A. The positive shift in the peak potential with increasing scan rate confirmed the irreversibility of CPF oxidation at poly($Na_2[Cu(HR)_4]$)/GCE (Fig. 8A).

The oxidation of CPF at poly(Na₂[Cu(HR)₄])/GCE is primarily a diffusion-controlled process, as indicated by the stronger correlation between peak current and the square root of the scan rate ($R^2 = 0.99588$) (Fig. 8C), compared to the correlation with the scan rate ($R^2 = 0.96741$) (Fig. 8B) [23]. The diffusion-controlled nature of the CPF oxidation process at poly(Na₂[Cu(HR)₄])/GCE is further supported by the slope of 0.61 in the log(I_P) versus log(ν) plot (Fig. 8D), which is close to the expected value of 0.50 for a fully diffusion-controlled process [23].

From the cyclic voltammetry data (Fig. 8A) at a scan rate of 100 mV s⁻¹, the number of electrons involved in CPF electrochemical oxidation at poly(Na₂[Cu(HR)₄])/GCE was determined. The value of αn was calculated using eq. 5, which relates the number of electrons (n) in an irreversible reaction to both the peak potential (Ep) and the half-wave potential (Ep,_{1/2}) [20].

$$E_p - E_{p1/2} = \frac{48.0}{an} \tag{5}$$

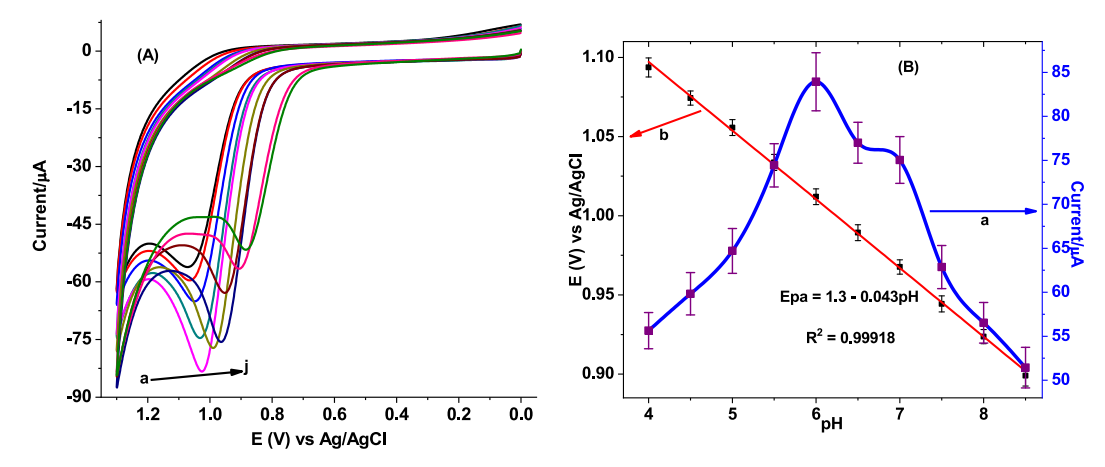


Fig. 7. (A) Cyclic voltammograms of poly(Na₂[Cu(HR)₄])/GCE in PBS at various pH values (a-j: 4.0, 4.5, 5.0, 5.5, 6.0, 6.5, 7.0, 7.5, 8.0, and 8.5, respectively) containing 0.5 mM CPF. (B) plot showing the average (a) peak potential and (b) peak current as a function of pH across the entire pH range.

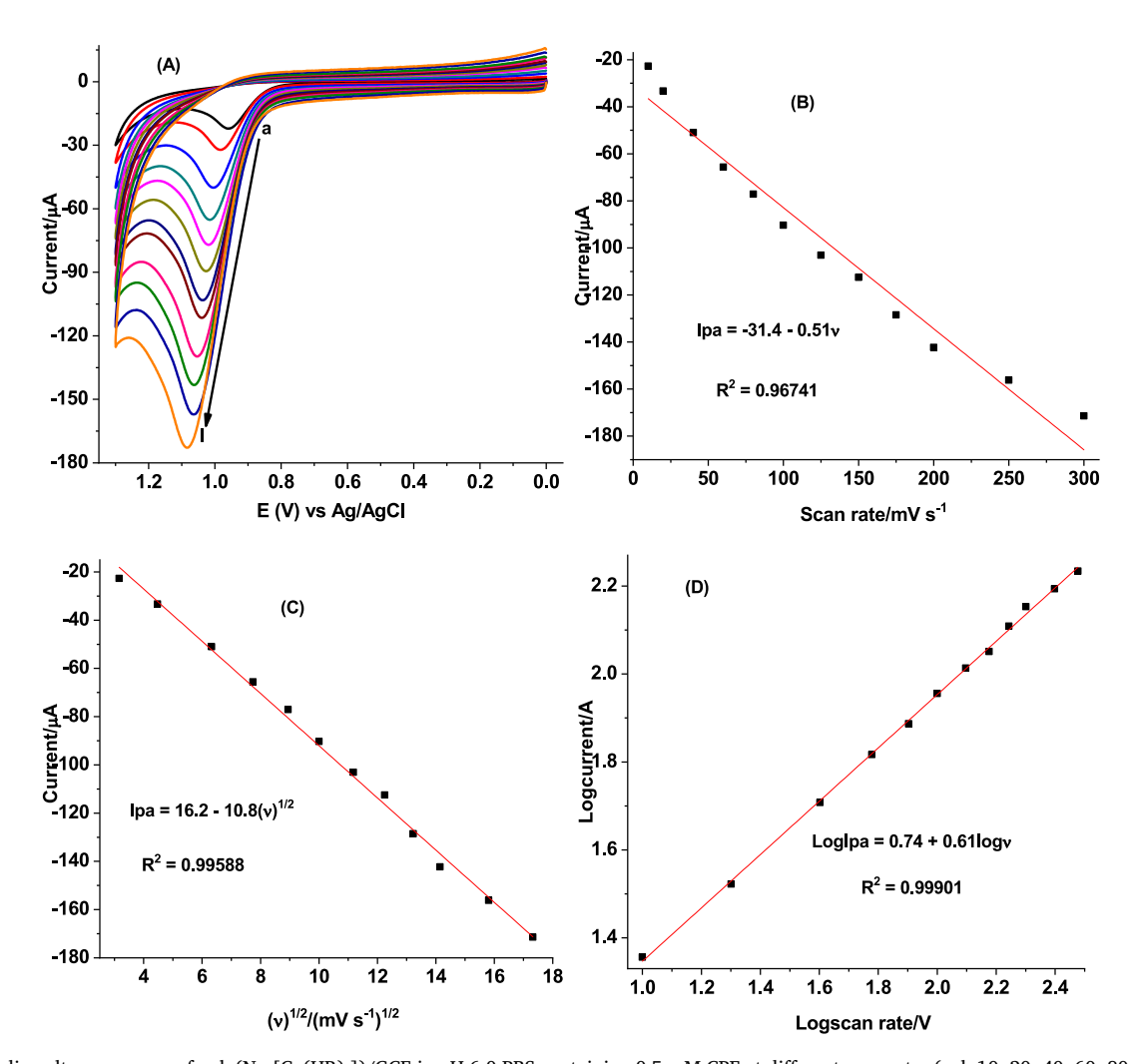


Fig. 8. (A) Cyclic voltammograms of poly(Na₂[Cu(HR)₄])/GCE in pH 6.0 PBS containing 0.5 mM CPF at different scan rates (a–l: 10, 20, 40, 60, 80, 100, 125, 150, 175, 200, 250, and 300 mV s⁻¹, respectively). Plots of (B) I_{P^0} vs. scan rate (ν), (C) I_{P^0} vs. $\nu^1/_2$, and (D) log I_{P^0} vs. $\log \nu$.

where $\boldsymbol{\alpha}$ is the charge transfer coefficient and \boldsymbol{n} is the number of electrons transferred.

From the cyclic voltammogram (Fig. 8A) at a scan rate of 100 mV s⁻¹, the peak potential (E_P) and half-peak potential (E_{P1/2}) were estimated to be 1017 mV and 963 mV, respectively and the value of αn was calculated as 0.89. Assuming α to be 0.5 for the irreversible electrode

process [24], the estimated number of electrons involved in the electrochemical oxidation of CPF at the poly(Na₂[Cu(HR)₄])/GCE surface was 1.78 (~2.0), which is in agreement with reported literatures [12]. Eq. 6 [19] was applied to determine α during the electrochemical oxidation of CPF at poly(Na₂[Cu(HR)₄])/GCE, which is based on the linear relationship between E_P and ln ν for the irreversible oxidation

process.

$$Ep = E^{\circ} + \frac{RT}{(1-\alpha)nF} \left\{ 0.780 + ln \left(\frac{D_R^{\frac{1}{2}}}{k^{\circ}} \right) + ln \left[\frac{(1-\alpha)nF\nu}{RT} \right]^{\frac{1}{2}} \right\}$$
 (6)

where E_{P} is the peak potential, E_{o} is the formal potential, α is the electron transfer coefficient, k_{o} is the electrochemical rate constant, T is the temperature (298 K), F is Faraday's constant, R is the gas constant, ν is the scan rate, and D represents the diffusion coefficient.

As shown in Fig. SM5, the slope value of 0.03 (slope = RT/[2(1 - α) nF] = 0.03) for the fitted line allowed for the calculation of n(1- α) at 25 °C, yielding a value of 0.91 using eq. (6). Assuming a two-electron process for CPF oxidation (calculated via eq. (5)), α was determined to be 0.545, which is close to the ideal value of 0.50 for an irreversible system. Based on these calculated kinetic parameters (n and α) and the proton-to-electron ratio (1:1), a reaction mechanism was proposed (Scheme 2), in agreement with previously reported literature [12].

3.7. DPV determination of CPF at poly(Na₂[cu(HR)₄])/GCE

Pulse techniques like differential pulse voltammetry (DPV) were chosen for CPF quantification in real samples due to their ability to reduce background currents, enhance sensitivity, and achieve lower detection limits compared to cyclic voltammetry [21,23]. As shown in Fig. 9, the oxidative peak current at poly(Na₂[Cu(HR)₄])/GCE was over eight times higher compared to that of the unmodified GCE, which is accompanied by a decrease in overpotential (Δ E \sim 131 mV), signifying the electrocatalytic effect of the poly(Na₂[Cu(HR)₄]) film towards CPF oxidation.

The DPV parameters, such as step potential and amplitude, were optimized to evaluate their influence on the oxidative peak current of CPF at poly(Na₂[Cu(HR)₄])/GCE while maintaining other conditions constant. Figure SM6 (A & B) shows the DPVs of poly(Na₂[Cu(HR)₄])/GCE in pH 6.0 PBS containing 0.5 mM CPF at varying step potentials and amplitudes, respectively. After evaluating the trade-off between enhancement of peak current and widening of peak shape, a step potential of 6 mV and a pulse amplitude of 75 mV were determined to be the optimal settings.

3.8. Calibration curve

Using the optimized solution and experimental conditions, the relationship between the oxidative peak current and varying concentrations of CPF was investigated via differential pulse voltammetry. Fig. 10 presents the background-corrected DPV responses for different CPF concentrations in pH 6.0 PBS at poly(Na₂[Cu(HR)₄])/GCE. As shown in the inset of Fig. 10, the oxidative peak current displayed a linear correlation with CPF concentration over the range of 0.01 to 400.0 μ M, with a correlation coefficient (R²) of 0.99974. Moreover, a detection limit (3 s/m) and a quantification limit (10s/m) were found to be 2.4 nM and 6.8 nM, respectively, where "s" represents the standard deviation of the blank (n = 7) and "m" is the slope of the regression. The low relative standard deviation (RSD) values with below 2.6 %, for triplicate current measurements of standard CPF solutions confirmed the precision of the proposed method.

Scheme 2. Proposed mechanism for CPF reaction

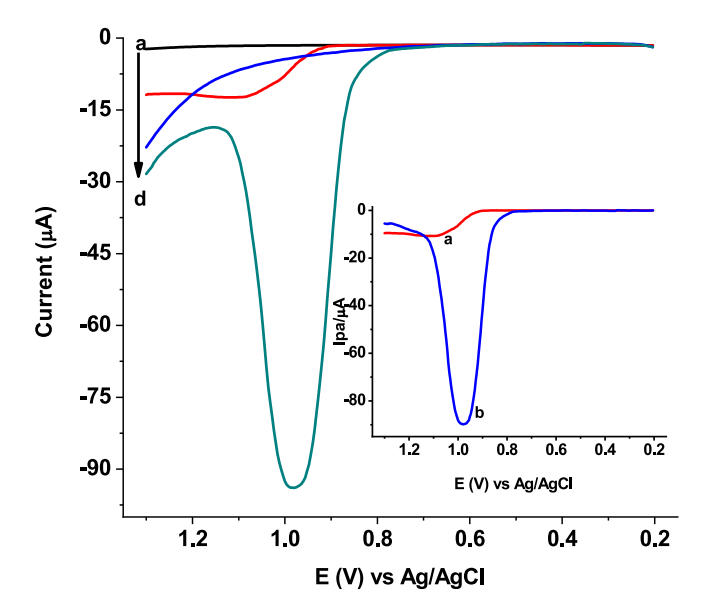


Fig. 9. DPVs of unmodified GCE (a & c) and poly(Na₂[Cu(HR)₄])/GCE (b & d) in pH 6.0 PBS containing no CPF (a & b) and 0.5 mM CPF (c & d). Inset: background corrected DPVs of a) bare GCE b) poly(Na₂[Cu(HR)₄])/GCE.

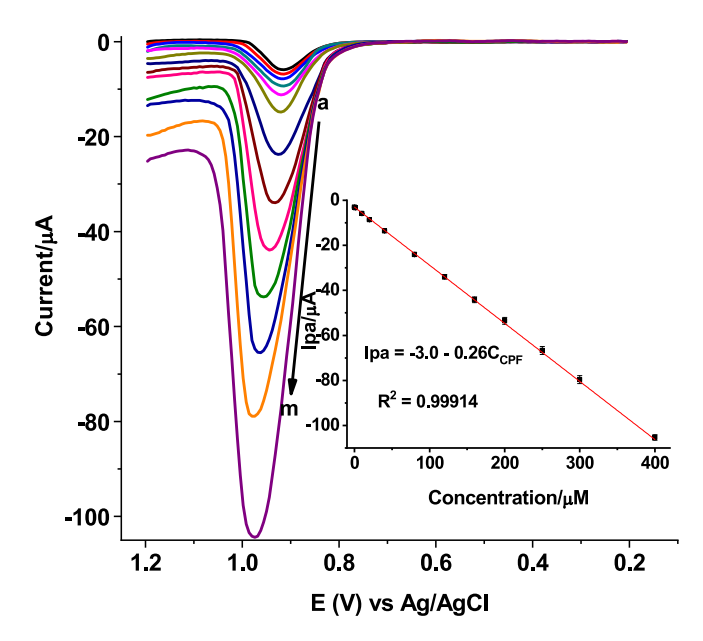


Fig. 10. Background-corrected DPVs for poly(Na₂[Cu(HR)₄])/GCE in pH 6.0 PBS were recorded for CPF concentrations of 0.01, 0.1, 1.0, 10.0, 20.0, 40.0, 80.0, 120.0, 160.0, 200.0, 250.0, 300.0, and 400.0 μ M (a–m, respectively) using a step potential of 6 mV and an amplitude of 75 mV. The inset shows a plot of Ipa (mean \pm %RSD) versus CPF concentration.

3.9. Stability studies

Tthe stability and reproducibility of the modified electrode for oxidation of CPF was studied using DPV measurements. This was carried out by recording seven consecutive DPVs of poly(Na₂[Cu(HR)₄])/GCE in pH 6.0 PBS with 0.5 mM CPF at an interval of two days for a two week period, with an error of 2.83 % \pm 1.37 (%RSD with triplicate measurement), demonstrating the reproducibility and stability of the developed method (Fig. SM7).

3.10. Application of the method for CPF analysis in real samples

The performance of the developed method for quantifying CPF using $poly(Na_2[Cu(HR)_4])/GCE$ was assessed using samples from three distinct brands of pharmaceutical tablets and biological fluids.

3.10.1. Tablet samples

To quantify the CPF content in tablet samples, three brands (Brucipro, Ciplet, and Cipro) were prepared according to the experimental protocol. The CPF content measured experimentally was then compared to the values declared by the manufacturer. The differential pulse voltammograms (DPVs) for CPF tablet samples with nominal concentrations of 20.0 and 40.0 μM for each brand are presented in Figure SM8.

Table 2 shows a summary of the CPF content measured in tablet samples using the calibration regression equation, with the results compared to the nominal values. The detected CPF concentrations for each sample was in the range of 98.05 % to 100.00 %, and the relative standard deviation (RSD) was below 2.9 %. This indicates that the established approach was accurate and the detected levels were relatively near to the expected quantity. The results showed that the established approach is effective for CPF determination in pharmaceutical formulations.

3.10.2. Cow milk sample

The established method was further utilized to detect CPF in milk samples prepared following the procedures described in the experimental section. The lack of a peak at the characteristic potential suggests the absence of CPF in the tested milk sample (curve a in Fig. 11).

3.10.3. Human blood serum sample

The lack of a peak at the characteristic potential of CPF (curve a of Fig. 12) suggests that CPF was not detected in the analyzed human blood serum sample. Two peaks observed at different potentials from that of CPF were identified, with peak-1 corresponding to uric acid and peak-2 to creatinine [25,26].

3.11. Method validation

To confirm the suitability of the newly developed poly(Na₂[Cu (HR)₄])/GCE method for CPF determination in real samples, including tablets, milk, and serum, spiked recovery tests, interference studies, and stability assessments were performed.

3.11.1. Spike recovery test

3.11.1.1. Cow milk sample. CPF recovery in spiked milk samples was

Table 2Summary of CPF content detected in tablet samples from various brands and the percent recovery relative to nominal values.

Tablet Labeled brand value (mg tablet)		Nominal amount in sample (µM)	Detected	Detected drug in	
			sample (μM) ^a	tablet (mg/ tablet)	%
Brucipro	500	20.0	19.69 ± 0.017	492.3	98.45
		40.0	$\begin{array}{c} 39.81 \; \pm \\ 0.019 \end{array}$	497.7	99.53
Ciplet	500	20.0	$19.61 \pm \\ 0.023$	490.3	98.05
		40.0	39.61 ± 0.029	495.2	99.03
Cipro	500	20.0	$\begin{array}{c} 20.00 \pm \\ 0.021 \end{array}$	500.0	100.00
		40.0	$\begin{array}{c} 40.00 \; \pm \\ 0.025 \end{array}$	500.0	100.00

 $^{^{\}rm a}$ Detected mean CPF \pm %RSD

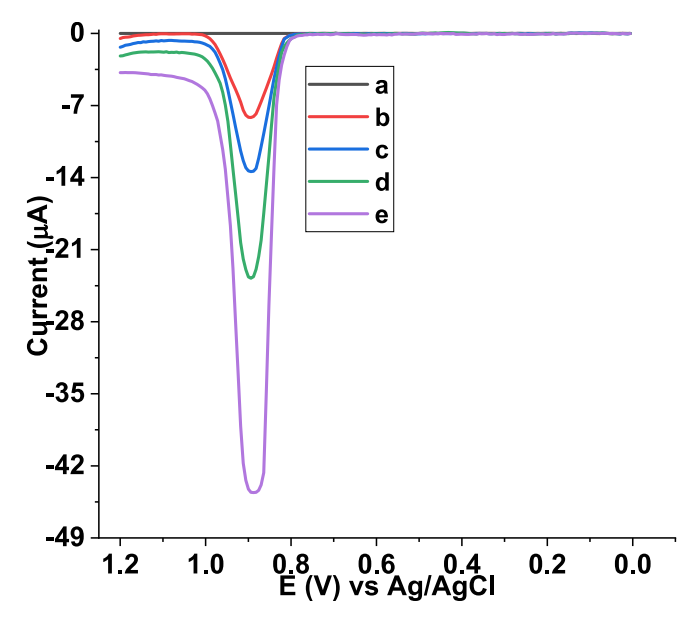


Fig. 11. Background-corrected DPVs of poly(Na₂[Cu(HR)₄])/GCE in pH 6.0 PBS for (a) unspiked milk, (b) milk $+20.0~\mu$ M CPF, (c) milk $+40.0~\mu$ M CPF, (d) milk $+80.0~\mu$ M CPF, and (e) milk $+160.0~\mu$ M CPF.

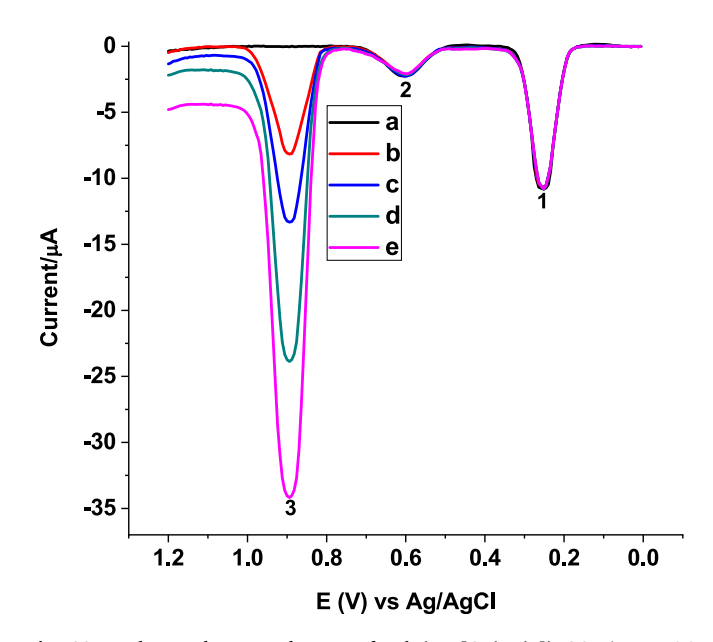


Fig. 12. Background-corrected DPVs of poly(Na₂[Cu(HR)₄])/GCE in pH 6.0 PBS for (a) unspiked serum, (b) serum $+20.0~\mu$ M CPF, (c) serum $+40.0~\mu$ M CPF, (d) serum $+80.0~\mu$ M CPF, and (e) serum $+120.0~\mu$ M CPF.

evaluated by adding 20.0, 40.0, 80.0, and 160.0 μ M of standard CPF (Fig. 11). The unspiked milk sample (curve a of Fig.11) showed no detectable peak, whereas a distinct peak corresponding to the characteristic potential of CPF appeared, with the current intensity increasing in direct relation to the amount of CPF added (curves b–e). The percent recovery of CPF in the spiked milk samples ranged from 99.40 % to 100.2 % (Table SM2), with a %RSD of less than 3.3 %, confirming the method's applicability for CPF determination in milk samples.

3.11.1.2. Human blood serum sample. To recover CPF from human blood serum, standard solutions of 20.0, 40.0, 80.0, and 120.0 μ M CPF were spiked into a pre-analyzed serum sample (Fig. 12). Irrespective of the amount of CPF spiked, the serum sample displayed peaks 1 and 2 at a potential that did not correspond to the characteristic potential of CPF,

and these peaks exhibited a constant current intensity, suggesting the presence of a non-CPF compounds. Upon spiking, new peaks (peak 3) emerged at the characteristic potential of CPF, and the intensity of these peaks increased with the amount of CPF spiked into the serum samples (curves b-e of Fig.12). The reliability of the established method was confirmed by Table 3, which demonstrates percent recoveries within the range of 99.25–100.0 %.

ND not detected, ^aDetected mean CPF \pm RSD.

3.11.1.3. Tablet samples. Standard CPF was spiked into tablet sample solutions in recovery trials to verify the correctness of the novel poly (Na₂[Cu(HR)₄])/GCE technique. For the recovery research, the previously explored Brucipro and Cipro pill sample solutions were supplemented with standard CPF solutions at concentrations of 0.0, 20.0, 40.0, and 80.0 μ M (Fig. SM9). The obtained excellent recovery rates, between 99.25 % and 100.40 % (Table SM3), validated that the devised approach was appropriate for CPF analysis in pharmaceutical tablet formulations.

3.11.2. Interference study

The selectivity of the developed method for CPF in biological fluid and pharmaceutical tablet samples in the presence of selected interferents was evaluated.

3.11.2.1. Blood serum sample. The method's selectivity to assess CPF in a serum sample with varying quantities of glucose (Glu) present was also examined (Fig. SM10). The method's selectivity was validated by the detection of CPF in a blood serum sample with an error of less than 3.42 %, even when different quantities of Glu were present (Table SM4).

3.11.2.2. Cow's milk sample. The effect of various concentrations of uric acid (UA) on the determination of CPF in cow's milk samples was investigated (Fig. 13). As shown in Table SM5, the spiked CPF in the milk sample was detected with a percentage error of less than 4.6 % in the presence of 10.0–80.0 μ M UA, demonstrating the selectivity of the method and validating it for CPF analysis in milk samples. Moreover, the addition of UA resulted in the appearance of a new peak (Fig.13) at exactly same potential as the signal for the serum sample (Fig.12), which increased proportionally with the amount of UA, further confirmed that peak-1 in serum samples corresponds to UA.

3.11.2.3. Pharmaceutical formulation sample. DPV measurements were conducted to assess the selectivity of poly(Na₂[Cu(HR)₄])/GCE for CPF detection in the company of potential interfering compounds, such as cloxacillin (CLOX), ampicillin (AMP), norfloxacin (NFN), chloroquine phosphate (CQP), and tinidazole (TDL). The effects of each interferent were studied at concentrations ranging from 0 to 80.0 μ M (Fig. SM11). Despite the presence of these interferents at varying concentrations, CPF could still be detected with an error of less than 4.30 % (Table SM6), demonstrating the specificity and precision of the proposed method for the precise identification of CPF.

3.12. Evaluation of the created sensor in relation to published techniques

To assess the performance of the sensor, we compared it with existing

Table 3 Recovery results of 20.0, 40.0, 80.0, and 120.0 μM CPF in spiked human serum samples.

Sample	Detected before spike (μM)	Spiked amount (µM)	Detected after spike (μM) ^a	Recovery (%)
Human	ND	20.0	19.85 ± 0.031	99.25
blood	ND	40.0	39.96 ± 0.035	99.90
serum	ND	80.0	79.62 ± 0.033	99.53
	ND	120.0	120.0 ± 0.030	100.0

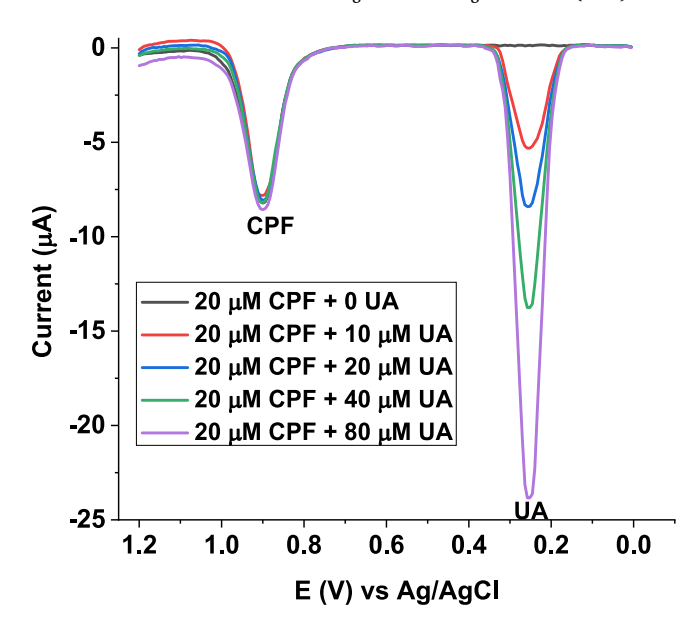


Fig. 13. Blank subtracted DPVs of pH 6.0 PBS containing 20.0 μ M CPF standard solution in the presence of various concentrations of UA (0.0, 10.0, 20.0, 40.0, & 80.0 μ M).

methods reported in the literature, considering factors such as substrate, modifier, linear range, and detection limit. Our approach, which involves a chip modifier and a simple modification process, showed exceptional performance, achieving the lowest detection limit and the widest linear dynamic range (see Table 4).

4. Conclusions

The successful preparation of the poly(Na₂[Cu(HR)₄]) modified GCE was confirmed through cyclic voltammetry and electrochemical impedance spectroscopy. The increased effective surface area, higher electrical conductivity, and increased surface roughness of poly(Na₂[Cu(HR)₄])/GCE are responsible for its improved electrocatalytic activity for CPF oxidation. The DPV method, utilizing the poly(Na₂[Cu(HR)₄])/GCE, was employed to determine CPF in blood samples and pharmaceutical formulations. The accuracy of this method was validated by the CPF content in the tablet samples, which ranged from 94.65 % to 100.00 % of the labeled amounts, using the optimized solution and DPV parameters. Excellent spike recovery rates, which varied from 99.25 % to 100.0 % for blood, 9.40 % to 100.2 % for milk, and 99.25 % to 100.40 % for tablet samples, further illustrated the method's reliability.

The current approach, based on poly(Na₂[Cu(HR)₄])/GCE, exhibited significant electrochemical advantages, including a wider linear range, lower detection limit, superior spike and interference recovery, and high sensor stability, all of which underscore its applicability. As a result, this technique shows promise for accurately measuring CPF across a spectrum of complex real samples, such as pharmaceutical tablets and biological fluids.

Funding

This research did not receive any direct funding from funding agencies.

CRediT authorship contribution statement

Adane Kassa: Writing – review & editing, Writing – original draft, Validation, Supervision, Software, Resources, Methodology, Investigation, Formal analysis, Data curation, Conceptualization. **Demisachew Shitaw:** Writing – review & editing, Writing – original draft, Validation,

Table 4Evaluation of the proposed method's performance against recently published selected works for CPF determination.

Electrode	Technique	Matrices	Dynamic range (μM)	LoD (μM)	Ref.
CZF-CME/CPE	AdSDPV	Tablet/blood serum and human urine	9.09–4700	0.0028	[12]
rGO/SPE	AdSDPV	Milk sample	1.0-8.0	0.3	[12]
CoFe ₂ O ₄₋ MWCNT/GCE	DPV	Tablet	0.1-1.0 & 1.0-30.0	0.036	[27]
Boron-doped diamond electrode	SWV	urine sample	2.5-50.0	2.46	[28]
MIP/GCE	DPV	Human serum & urine	50-5000	12.0	[29]
(Ca ₁₀ (PO ₄) ₆ (OH) ₂) sub-MPs/GCE	SWV	Tablet and biological sample	0.01-1310.0	0.0918	[30]
f-MWCNT@Poly-Aniline/GCE	LSV	Tablet formulations	0.1 1.0 & 1.0-20.0	0.08	[31]
mag@MIP-CB-NF/SPE	DPV	River water & synthetic urine	0.5–7.0	0.0084	[32]
Poly(Na ₂ [Cu(HR) ₄])/GCE	DPV	Tablet/blood serum and human urine	0.01-400.0	0.002	This work

Software, Resources, Methodology, Investigation, Formal analysis, Data curation. **Zelalem Bitew:** Writing – review & editing, Writing – original draft, Validation, Software, Resources, Methodology, Investigation, Formal analysis, Data curation. **Atakilt Abebe:** Writing – review & editing, Writing – original draft, Validation, Supervision, Software, Resources, Methodology, Investigation, Formal analysis, Data curation, Conceptualization.

Declaration of competing interest

The authors guarantee that none of the work presented in this paper may have been impacted by any known financial conflicts of interest or personal relationships.

Acknowledgements

The authors express their gratitude to Addis Pharmaceutical Factory (APF), Debre Markos University, the College of Science at Bahir Dar University, and the Ethiopian Food and Drug Administration Authority (EFDA) for their generous support in providing standards and laboratory facilities.

Appendix A. Supplementary data

Supplementary data to this article can be found online at https://doi.org/10.1016/j.sbsr.2025.100825.

Data availability

No data was used for the research described in the article.

References

- D.O. Guimarães, L.D.S. Momesso, M.T. Pupo, Antibiotics: therapeutic importance and perspectives for the discovery and development of new agents, Química Nova 33 (2010) 667–679, https://doi.org/10.1590/S0100-40422010000300035.
- [2] A. Rehman, W.M. Patrick, I.L. Lamont, Mechanisms of ciprofloxacin resistance in Pseudomonas aeruginosa: new approaches to an old problem, J. Med. Microbiol. 68 (1) (2019) 1–10, https://doi.org/10.1099/jmm.0.000873.
- [3] D.M. Campoli-Richards, J.P. Monk, A. Price, P. Benfield, P.A. Todd, A. Ward, Ciprofloxacin: a review of its antibacterial activity, pharmacokinetic properties and therapeutic use, Drugs 35 (1988) 373–447, https://doi.org/10.2165/00003495-198835040-00003.
- [4] M.H. El Demeiry, S. Emara, Y. Abuleila, A. Ali, G. Hadad, R. Abdel Salam, A review article on ciprofloxacin determination with various analytical techniques, Records Pharm. Biomed. Sci. 5 (Chemistry) (2021) 28–32.
- [5] K. Elgendy, M. Zaky, T.A. Eldin, S. Fadel, Rapid HPLC determination of ciprofloxacin, ofloxacin, and marbofloxacin alone or in a mixture, Resul. Chem. 5 (2023) 100749, https://doi.org/10.1016/j.rechem.2022.100749.
- [6] T.Y. Mahmoud, I.S. Hamza, A.L. Jarallah, Spectrophotometric method for the determination of ciprofloxacin in pure and pharmaceutical preparations: development and validation, Eng. Proceed. 59 (1) (2024) 164, https://doi.org/ 10.3390/engproc2023059164.
- [7] M.K. Matta, A. Chockalingam, A. Gandhi, S. Stewart, L. Xu, K. Shea, R. Rouse, LC-MS/MS based quantitation of ciprofloxacin and its application to antimicrobial resistance study in Balb/c mouse plasma, urine, bladder and kidneys, Anal. Methods 10 (10) (2018) 1237–1246, https://doi.org/10.1039/C7AY02923C.
- [8] A. Kassa, G.T. Tigineh, A. Abebe, Electrochemical determination of chloroquine phosphate in real samples using a Diresorcinate-1, 10-phenanthrolinecobalt (II)-

- modified glassy carbon electrode, ChemistryOpen 12 (3) (2023) e202300004, https://doi.org/10.1002/open.202300004.
- [9] R.D. Crapnell, P.S. Adarakatti, C.E. Banks, Electroanalytical overview: the measurement of ciprofloxacin, Sensors & Diagnostics 3 (1) (2024) 40–58, https://doi.org/10.1039/D3SD00129F.
- [10] M. Xu, H. Ma, J. Song, Polarographic behavior of cephalexin and its determination in pharmaceuticals and human serum, J. Pharm. Biomed. Anal. 35 (5) (2004) 1075–1081, https://doi.org/10.1016/j.jpba.2004.03.018.
- [11] R. Chauhan, A.A. Gill, Z. Nate, R. Karpoormath, Highly selective electrochemical detection of ciprofloxacin using reduced graphene oxide/poly (phenol red) modified glassy carbon electrode, J. Electroanal. Chem. 871 (2020) 114254, https://doi.org/10.1016/j.jelechem.2020.114254.
- [12] M.P. Kingsley, P.K. Kalambate, A.K. Srivastava, Simultaneous determination of ciprofloxacin and paracetamol by adsorptive stripping voltammetry using copper zinc ferrite nanoparticles modified carbon paste electrode, RSC Adv. 6 (18) (2016) 15101–15111, https://doi.org/10.1039/C5RA19861E.
- [13] M. Pan, P. Guo, H. Liu, J. Lu, Q. Xie, Graphene oxide modified screen-printed electrode for highly sensitive and selective electrochemical detection of ciprofloxacin residues in milk, J. Anal. Sci. Technol. 12 (1) (2021) 55.
- [14] N. Gissawong, S. Srijaranai, S. Boonchiangma, P. Uppachai, K. Seehamart, S. Jantrasee, S. Mukdasai, An electrochemical sensor for voltammetric detection of ciprofloxacin using a glassy carbon electrode modified with activated carbon, gold nanoparticles and supramolecular solvent, Microchim. Acta 188 (6) (2021) 208, https://doi.org/10.1007/s00604-021-04869-z.
- [15] A. Kassa, A. Abebe, G. Tamiru, M. Amare, Synthesis of a novel [diresorcinate-1, 10-phenanthrolinecobalt (II)] complex, and Potentiodynamic fabrication of poly (DHRPCo)/GCE for Selective Square wave Voltammetric determination of procaine penicillin G in pharmaceutical and biological fluid samples, ChemistrySelect 7 (1) (2022) e202103458, https://doi.org/10.1002/slct.202103458.
- [16] A. Kassa, M. Amare, A. Benor, G.T. Tigineh, Y. Beyene, M. Tefera, A. Abebe, Potentiodynamic poly (resorcinol)-modified glassy carbon electrode as a voltammetric sensor for determining cephalexin and cefadroxil simultaneously in pharmaceutical formulation and biological fluid samples, ACS Omega 7 (38) (2022) 34599–34607, https://doi.org/10.1021/acsomega.2c04514.
- [17] M.T. Ayana, B.B. Beyene, G.T. Tigineh, A. Abebe, A novel homobinuclear copper (II) complex with resorcinolate: synthesis, characterization and assessment of antibacterial activity, Chem. Afr. 6 (1) (2023) 267–273, https://doi.org/10.1007/ s42250-022-00517-y.
- [18] T. Tsega, G. Chanie, A. Kassa, M. Gebrezgiabher, D. Tesfaye, M. Metto, A. Abebe, Synthesis, structural characterisations, electrochemical behavior and antibacterial activities of a chromium (III) resorcinolate complex, Int. J. Electrochem. Sci. 19 (8) (2024) 100659, https://doi.org/10.1016/j.ijoes.2024.100659.
- [19] P.W. Atkins, J. De Paula, J. Keeler, Atkins' Physical Chemistry, Oxford university press, 2023.
- [20] A.J. Bard, L.R. Faulkner, H.S. White, Electrochemical Methods: Fundamentals and Applications, John Wiley & Sons, 2022.
- [21] A. Kassa, A. Abebe, M. Amare, Synthesis, characterization, and electropolymerization of a novel cu (II) complex based on 1, 10-phenanthroline for electrochemical determination of amoxicillin in pharmaceutical tablet formulations, Electrochim. Acta 384 (2021) 138402, https://doi.org/10.1016/j. electacta.2021.138402.
- [22] M.E. Draz, D. El Wasseef, N. El Enany, M.E. Wahba, Green approach for tracking the photofate of ciprofloxacin and levofloxacin in different matrices adopting synchronous fluorescence spectroscopy: a kinetic study, R. Soc. Open Sci. 10 (1) (2023) 221086, https://doi.org/10.1098/rsos.221086.
- [23] A. Kassa, M. Amare, Highly selective and sensitive differential pulse voltammetric method based on poly (alizarin)/GCE for determination of cefadroxil in tablet and human urine samples, Arab. J. Chem. 14 (8) (2021) 103296, https://doi.org/ 10.1016/j.arabic.2021.103296.
- [24] E. Laviron, General expression of the linear potential sweep voltammogram in the case of diffusionless electrochemical systems, J. Electroanal. Chem. Interfacial Electrochem. 101 (1) (1979) 19–28.
- [25] T. Fukuda, H. Muguruma, H. Iwasa, T. Tanaka, A. Hiratsuka, T. Shimizu, K. Tsuji, T. Kishimoto, Electrochemical determination of uric acid in urine and serum with uricase/carbon nanotube/carboxymethylcellulose electrode, Anal. Biochem. 590 (2020) 113533. https://doi.org/10.1016/j.ab.2019.113533.
- [26] E. Fava, do Prado, T., Garcia-Filho, A., Silva, T., Cincotto, F., de Moraes, F., Faria, R., & Fatibello-Filho, O., Non-enzymatic electrochemical determination of creatinine using a novel screen-printed microcell, Talanta 207 (2020) 120277, https://doi.org/10.1016/j.talanta.2019.120277.

- [27] A. Hosseini, E. Sohouli, M. Gholami, A. Sobhani-Nasab, S.A. Mirhosseini, Electrochemical determination of ciprofloxacin using glassy carbon electrode modified with CoFe₂0₄-MWCNT, Anal. Bioanal. Electrochem. 11 (8) (2019) 096–1008
- [28] G.S. Garbellini, R.C. Rocha-Filho, O. Fatibello-Filho, Voltammetric determination of ciprofloxacin in urine samples and its interaction with dsDNA on a cathodically pretreated boron-doped diamond electrode, Anal. Methods 7 (8) (2015) 3411–3418, https://doi.org/10.1039/C5AY00625B.
- [29] B.G. Akyüz, S.P. Özkorucuklu, E. Kır, G.Y. Baştemur, Determination of ciprofloxacin in pharmaceutical dosage, human serum and urine, using molecularly imprinted polymer modified electrode by voltammetry, Avrupa Bilim ve Teknoloji Dergisi 20 (2020) 859–865, https://doi.org/10.31590/ejosat.796654.
- [30] S. Anitta, C. Sekar, Voltammetric determination of paracetamol and ciprofloxacin in the presence of vitamin C using cuttlefish bone-derived hydroxyapatite submicroparticles as electrode material, Resul. Chem. 5 (2023) 100816, https://doi. org/10.1016/j.rechem.2023.100816.
- [31] P. Jain, R.V. Motghare, Electro-oxidation and determination of ciprofloxacin at f-mwcnt@ poly-aniline glassy carbon electrode, J. Electrochem. Soc. 169 (5) (2022) 056515
- [32] A. Wong, M. Santos, A., A. Silva, T., Moraes, F. C., Fatibello-Filho, O., & Sotomayor, M. D., Sensitive and selective Voltammetric determination of ciprofloxacin using screen-printed electrodes modified with carbon black and magnetic-molecularly imprinted polymer, Electroanalysis 35 (1) (2023) e202200165, https://doi.org/10.1002/elan.202200165.